

# LOW-PASS FILTERING EFFECTS OF VISCOUS SUBLAYER ON HIGH SCHMIDT NUMBER MASS TRANSFER CLOSE TO A SOLID WALL

*Y. Hasegawa and N. Kasagi*

*Department of Mechanical Engineering, The University of Tokyo,*

*7-3-1 Hongo, Bunkyo-ku, Tokyo, Japan, 113-8656*

[hasegawa@thtlab.t.u-tokyo.ac.jp](mailto:hasegawa@thtlab.t.u-tokyo.ac.jp)

## Abstract

Numerical simulation of high Schmidt number turbulent mass transfer across a solid wall is carried out. Particular attention is paid to damping of high-frequency concentration fluctuations close to a solid wall and its effects on the mass transfer mechanism. Spatio-temporal correlation shows that the high Schmidt number concentration field becomes less sensitive to the normal velocity fluctuations inside the viscous sublayer. As a result, only lower-frequency velocity fluctuations penetrate the viscous sublayer, and control the mass transfer. This would be a primary reason why the analogy between momentum and mass transfer, which has been widely used in engineering applications, does not hold at high Schmidt numbers.

## 1 Introduction

Turbulent high Schmidt number scalar transfer across a solid wall plays important roles in a variety of engineering applications, such as water-cooling system in internal-combustion engines. In addition, it is known that the mass transfer mechanism across a highly contaminated air-water interface is essentially the same as that near a solid wall (Hasegawa and Kasagi, 2008). Hence, the understanding and modelling of transport processes near a solid wall are important issues not only in engineering, but also in environmental problems.

When considering the high Schmidt number mass transfer, the concentration boundary layer becomes much thinner than the momentum boundary layer, so that the transport mechanism is governed by turbulent motions in the immediate vicinity of a wall. Therefore, Taylor series expansion has been widely employed for representation of velocity and concentration fields. Considering that both the eddy diffusivity  $E_d$  and eddy viscosity  $E_v$  are proportional to the cube of the distance from a wall, the analogy between momentum and mass transfer has been well documented (Monin and Yaglom, 1971; Kader, 1981). This leads to a well-known relationship  $Q \propto Sc^{-2/3}$ , where  $Q$  is the mass transfer rate.

However, according to precise experiments with electrochemical techniques conducted by Shaw and

Hanratty (1977),  $Q$  is proportional to  $Sc^{-0.704}$ . Although this discrepancy in the Schmidt number exponent might be considered trivial, it results in 20 % difference in the mass transfer rate at  $Sc = 1000$ , which is the typical value of a gaseous solute in water. In addition, the deviation of the Schmidt number exponent from  $-2/3$  suggests the change in the transport mechanism at high Schmidt numbers.

Recently, numerical simulations of high Schmidt number mass transfer have been carried out by several groups (Na and Hanratty, 2000; Seki, et al., 2006; Bergant and Tiselj, 2007; Hasegawa and Kasagi, 2007). These data commonly show that the turbulent Schmidt number, which is defined by  $Sc_t = E_v / E_d$ , is increased with the Schmidt number in the vicinity from the wall. In addition, the high-frequency concentration fluctuations at high Schmidt numbers are strongly damped inside the viscous sublayer (Hasegawa and Kasagi, 2007). In other words, the viscous sublayer acts as something like a low-pass filter, so the concentration field responds to only low-frequency velocity fluctuations. These results indicate that the analogy between the momentum and mass transfer can not be used for predicting the mass transfer.

In the present study, we carry out numerical simulation of turbulent mass transfer at high Schmidt numbers. The Schmidt number is systematically changed as  $Sc = 1.0, 100, 200$  and  $400$ . Our objective is to clarify how the damping of high-frequency fluctuations influences the concentration statistics and the mass transfer mechanisms inside the viscous sublayer. These will provide useful information in establishing the scaling-law of the concentration boundary layer and developing the mass transfer model.

## 2 Computational Model

The computational domain and coordinate system considered in the present study are shown in Fig. 1, where  $x, y$  and  $z$  are streamwise, wall-normal and spanwise directions, respectively. The flow is driven by constant pressure gradient in the streamwise direction. A no-slip condition is imposed at the top boundary, while a free-slip at the bottom boundary. For the concentration field, constant concentrations,

i.e.,  $c = 1.0$  and  $0$  are applied at the top and bottom boundary, respectively. The computational periods are chosen to be  $2.5 \pi \delta^*$  and  $\pi \delta^*$  in  $x$  and  $z$  directions, respectively, where  $\delta^*$  is the depth of the channel. A value with an asterisk represents a dimensional value throughout the present paper.

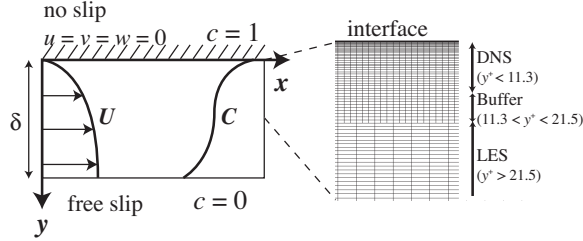


Figure 1: Computational domain and coordinate system

The governing equations are the incompressible Navier-Stokes, continuity and scalar transport equations given below:

$$\frac{\partial u_i}{\partial t} + u_j \frac{\partial u_i}{\partial x_j} = -\frac{\partial p}{\partial x_i} + \frac{1}{Re_\tau} \frac{\partial^2 u_i}{\partial x_j \partial x_j}, \quad (1)$$

$$\frac{\partial u_i}{\partial x_i} = 0, \quad (2)$$

$$\frac{\partial c}{\partial t} + u_j \frac{\partial c}{\partial x_j} = \frac{1}{Sc Re_\tau} \frac{\partial^2 c}{\partial x_j \partial x_j}, \quad (3)$$

where, the velocity  $u_i$  and the coordinate  $x_i$  are non-dimensionalized by  $u_\tau^*$  and  $\delta^*$  in each phase, where  $u_\tau^*$  is the friction velocity at the top wall. The concentration  $c^*$  of a solute is normalized by the concentration difference  $\Delta C^*$  between the top and bottom boundaries. The non-dimensional parameters which characterize the velocity and concentration fields are the Reynolds number  $Re_\tau = u_\tau^* \delta^* / \nu^*$  and the Schmidt number  $Sc = \nu^* / D^*$ , where  $\nu^*$  and  $D^*$  are the kinematic viscosity of fluid and the molecular diffusivity of a gaseous solute, respectively. In the present study, the Reynolds number is kept constant as  $Re_\tau = 150$ , while the Schmidt number is systematically changed as  $Sc = 1.0, 100, 200$  and  $400$ .

Direct numerical simulation (DNS) is applied to the velocity and concentration fields at  $Sc = 1.0$  by using a pseudo-spectral method.  $64 \times 64$  Fourier modes in the  $x$  and  $z$  directions and Chebyshev polynomials up to 144 are used. For high Schmidt numbers from 100 to 400, we apply a hybrid DNS/LES scheme, which employs DNS with high-resolution grids within the thin concentration boundary layer, while large eddy simulation (LES) with coarser grids for the outer regions. We provide a switching region between them in order to connect the two regions smoothly. The DNS region is determined as  $y^+_{DNS} < 11.3$  so that the more than 95 % of the mean concentration change is resolved by DNS. The number of grids employed in each region are listed in Table 1. By introducing such a solu-

tion-adaptive scheme, we can calculate the high Schmidt number concentration field with reasonable cost, while maintaining accuracy near the wall. The details of the hybrid DNS/LES scheme and its verification can be found in Hasegawa and Kasagi (2007).

Table 1: Number of modes and grids in hybrid DNS/LES

Sc	Region	$k_x, N_y, k_z$	$\Delta x^+$	$\Delta y^+$	$\Delta z^+$
100	DNS	192, 34, 192	6.1	0.01 ~ 0.62	2.4
	Switching	192, 15, 192	6.1	0.66 ~ 0.85	2.4
	LES	64, 144, 64	184	0.01 ~ 0.79	7.2
200	DNS	256, 34, 256	4.6	0.01 ~ 0.62	1.8
	Switching	256, 15, 256	4.6	0.66 ~ 0.85	1.8
	LES	64, 144, 64	184	0.01 ~ 0.79	7.2
400	DNS	288, 40, 288	4.1	0.008 ~ 0.58	1.6
	Switching	288, 15, 288	4.1	0.60 ~ 0.77	1.6
	LES	64, 162, 64	184	0.008 ~ 0.77	7.2

### 3 High Schmidt number effects on Concentration Statistics

The global mass transfer rate  $Q^+$  is defined as:

$$Q^+ = \frac{Q^*}{u_\tau^* (C_T^* - C_B^*)} = \frac{1}{\Delta C_B^+}, \quad (4)$$

Here,  $C_T^*$  and  $C_B^*$  are the mean concentrations at the top wall and the bulk, respectively, while  $\Delta C_B^+ = C_T^* - C_B^*$ . It is known that the Schmidt number dependency of the mass transfer rate changes around  $Sc = 10$ . Namely, the DNS data obtained by Na et al. (1999) up to  $Sc = 10$  leads to  $Q^+ = 0.0509 \times Sc^{-0.546}$ . In contrast, the laboratory measurement by Shaw and Hanratty (1977a) and the Lagrangian calculation by Na et al. (1999) can be correlated with  $Q^+ = 0.0889 \times Sc^{-0.704}$  for higher Schmidt numbers. The present results show good agreement with the two correlations as shown in Fig. 2. Note that the present results agree with the previous data that the mass transfer rate decreases faster than  $Sc^{-2/3}$  at high Schmidt numbers.

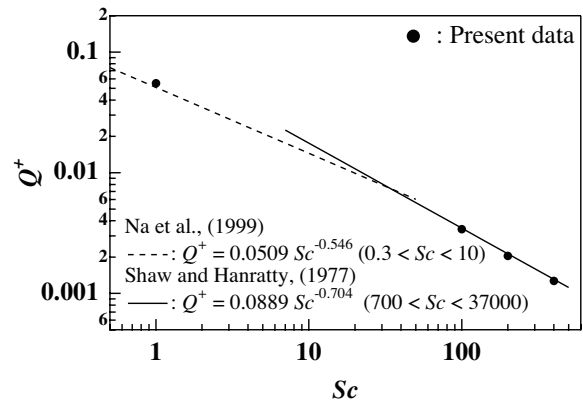


Figure 2: Mass transfer rate as a function of the Schmidt number

The mean concentration profiles near a solid wall are shown in Fig. 3. The abscissa is the distance from the top wall in the shear unit. The ordinate is the mean concentration relative to the concentration at the top wall non-dimensionalized by the friction concentration  $c_\tau^*$ , where  $c_\tau^* = Q^*/u_\tau^*$  and  $Q^*$  is mean mass flux at a solid wall. Obviously, the concentration boundary layer becomes thinner with increasing the Schmidt number. The thickness of the diffusive sublayer  $\delta_c^+$ , where  $C^+ = Sc \cdot y^+$  is satisfied within deviation of 5 %, is plotted as a function of the Schmidt number in Fig. 4. By assuming the analogy between the momentum and mass transfer, we obtain a conventional scaling law, i.e.,  $\delta_c^+ \propto Sc^{-1/3}$ . In contrast, recent DNS data obtained by Schwertfirm and Manhart (2007) show that  $\delta_c$  varies as  $\delta_c^+ \propto Sc^{-0.29}$ . The present data support the latter correlation as shown in Fig. 4, while conflict with the conventional scaling law.

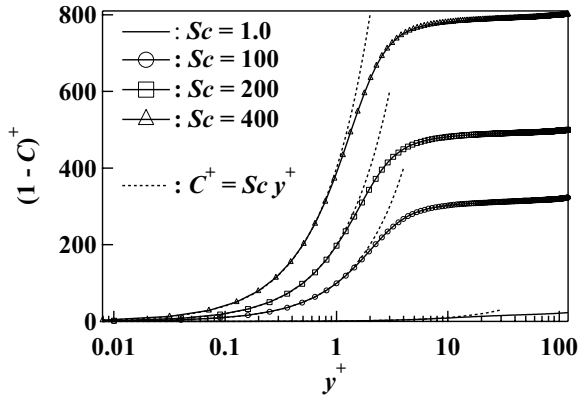


Figure 3: Mean concentration profiles.

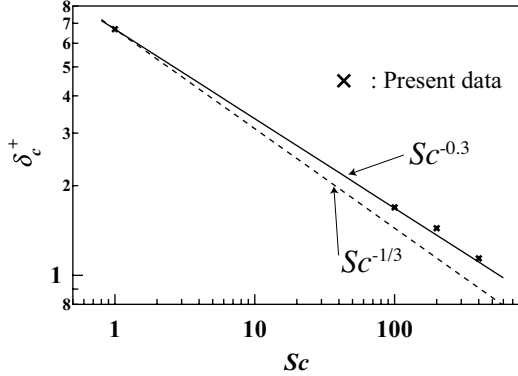


Figure 4: Schmidt number dependency of the diffusive sublayer thickness.

In Fig. 5, the concentration fluctuations non-dimensionalized by the concentration difference  $\Delta C_B$  between the top wall and the bulk are shown. In accordance with the scaling of the diffusive sublayer thickness shown in Fig. 4, the abscissa is the distance from the wall multiplied by  $Sc^{0.3}$ . The profile at  $Sc = 1.0$  deviates from the other data. This is mainly because the concentration boundary layer extends beyond the viscous sublayer. In contrast, At high Schmidt numbers, the peak of  $c_{rms}$  locates well within

the viscous sublayer, and the profiles converge to a single line.

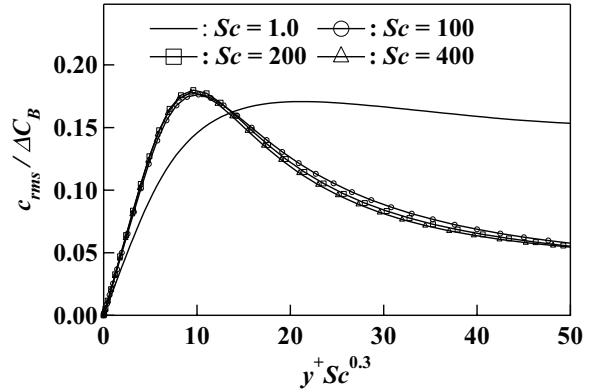


Figure 5: Concentration fluctuations

The eddy diffusivity  $E_d$  and eddy viscosity  $E_v$  are defined as follows:

$$E_d^+ = \overline{c^+ v^+} \left( \frac{dC^+}{dy^+} \right)^{-1} \quad (5)$$

$$E_v^+ = -\overline{u^+ v^+} \left( \frac{dU^+}{dy^+} \right)^{-1} \quad (6)$$

Considering the limiting behavior of velocity and concentration fluctuations toward a solid wall, it is shown that both  $E_d$  and  $E_v$  vary as  $y^3$  in the immediate vicinity from the wall (Hasegawa and Kasagi, 2007). In Fig. 6, the limiting behavior of  $E_d$  and  $E_v$  are shown.  $E_d$  at  $Sc = 1.0$  coincide with  $E_v$ , and they are proportional to  $y^3$  near a solid wall. In contrast,  $E_d$  at high Schmidt numbers decreases faster than  $y^3$  near a solid wall. It is known that the region where  $E_d^+ \propto y^{+3}$  always lies in the diffusive sublayer, where the molecular diffusion is dominant over the turbulent transport (Na et al., 1999; Hasegawa and Kasagi, 2007). Based on laboratory measurement, Shaw and Hanratty (1977a) argue that  $E_d$  over the concentration boundary layer is better represented by the  $E_d^+ = 0.000463y^{+3.38}$  for high Schmidt numbers. The present results agree fairly well with the correlation.

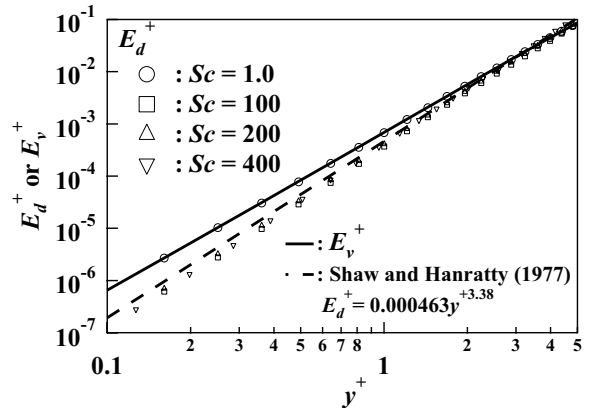


Figure 6: Limiting behavior of eddy diffusivity and eddy viscosity close to the wall

The turbulent Schmidt number  $Sc_t$  is defined as:

$$Sc_t = \frac{E_v^+}{E_d^+}. \quad (7)$$

In Fig. 7, the limiting behavior of  $Sc_t$  is shown. For all cases,  $E_d$  is almost constant and close to unity outside the viscous sublayer  $y^+ > 5$ . High Schmidt number effects appear close to the wall. Specifically,  $Sc_t$  increases as the wall is approached, and the limiting value is monotonically increased with the Schmidt numbers. Although further computation with finer grids is necessary to obtain the exact limiting value of  $Sc_t$  at the wall, it is clear that the assumption of constant  $Sc_t$  inside the concentration boundary layer, in other words, the analogy between the momentum and mass transfer cannot be used in predicting the mass transfer rate at high Schmidt numbers. The drastic change of  $Sc_t$  close to the wall suggests the changes in the mass transfer mechanism. In the following sections, we focus on the response of the concentration boundary layer to the velocity fluctuation inside the viscous sublayer.

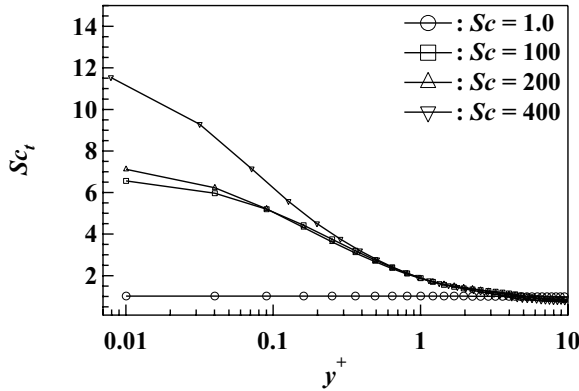


Figure 7: Turbulent Schmidt number

#### 4 Frequency characteristics of high Schmidt number concentration field.

Because of a thin concentration boundary layer at the high Schmidt number, the transport equation (3) of the solute concentration can be simplified as:

$$\frac{\partial c}{\partial t^+} + v^+ \frac{\partial c}{\partial y^+} = \frac{1}{Sc} \frac{\partial^2 c}{\partial y^{+2}}. \quad (8)$$

Since the wall shear governs the near-wall turbulence and associated transport phenomena,  $v$  and  $y$  in Eq. (8) are non-dimensionalized by the friction scales, while the concentration is normalized by  $\Delta C_B^*$ . Inside the viscous sublayer,  $v$  can be approximated by  $v(x, y, z, t) = \gamma(x, z, t)y^2$ , where  $2\gamma = (\partial^2 v / \partial y^2)_{y=0}$ .

Shaw and Hanratty (1977b) derived the following relationship for high frequencies:

$$\frac{W_q(\omega)}{Q^2} = \frac{4W_\gamma(\omega)}{Sc\omega^3}. \quad (9)$$

Here,  $W_q$  and  $W_\gamma$  are the frequency spectra of the local mass transfer rate  $q = (1/Sc)(\partial c / \partial y)_{y=0}$  and  $\gamma$ , respectively. Good agreement between the present

data and the model prediction by Eq. (9) is confirmed. Equation (9) explains fundamental features of concentration fluctuations close to the wall. Specifically, the high-frequency concentration fluctuations attenuate in inverse proportion to the cube of the frequency  $\omega$ . In addition, the appearance of  $Sc$  in the denominator of Eq. (9) results in the strong damping at the high Schmidt number.

Recently, Hasegawa and Kasagi (2007) show that the damping of concentration fluctuation has a strong impact on the transport mechanism close to the wall. Specifically, the contribution of high-frequency fluctuations to the co-spectrum of wall-normal turbulent mass flux  $\overline{c'v'}$  drastically reduced at the high Schmidt number. This indicates that low-frequency velocity fluctuations, which possess only a small fraction of total kinetic energy, govern the mass transfer.

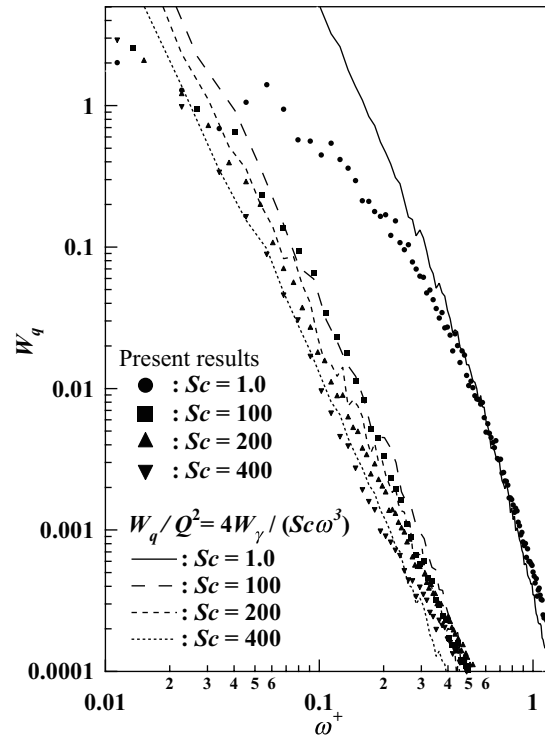


Figure 8: Frequency spectra of local mass transfer rate

#### 5 Spatio-temporal correlation between velocity and concentration fields.

In order to clarify high Schmidt number effects on the mass transfer, the spatio-temporal correlation coefficients between the normal velocity at  $y_0^+$  away from the wall and velocity/concentration fluctuations are calculated:

$$R_\alpha(y, \Delta t) = \frac{\overline{\alpha'(x, y, z, t)v'(x, y_0, z, t)}}{\alpha_{rms}(y)v_{rms}(y_0)}. \quad (10)$$

Here,  $\alpha$  denotes a velocity component or concentration. In Fig. 9,  $R_\alpha$  when  $y_0^+ = 12$ , are plotted. In response to the upwelling motion toward the top wall at  $\Delta t^+ = 0$ , i.e.  $R_v > 0$ , low concentration and high

streamwise velocity fluctuations are induced, i.e.,  $R_c < 0$  and  $R_u > 0$ . In the case of  $Sc = 1.0$ , the concentration field quickly responds to the normal velocity fluctuation even close to the wall. It should be also noted that  $R_u$  has an opposite sign, but strong similarity to  $R_c$ . In contrast, at  $Sc = 100$ , concentration field becomes less sensitive to the velocity fluctuation close to the wall. As the wall is approached, the peak value of  $R_c$  decreases. In addition, there exists large temporal difference in the response of the concentration field. Specifically,  $R_c$  at  $Sc = 100$  has a peak around  $\Delta t^+ = 35$  after the normal velocity is induced.

In order to clarify the Schmidt number dependency on the response of the concentration field to the normal velocity fluctuation  $v'$ , the spatio-temporal correlation  $R_q$  between  $v'$  at  $y_0^+ = 12$  and the local mass transfer rate  $q$  is shown in Fig. 10. It is found that the local mass transfer rate becomes less sensitive to the normal velocity fluctuation, and the response time  $\Delta T_q^+$  is increased with increasing the Schmidt number. In Fig. 11,  $\Delta T_q^+$  is plotted as a function of the Schmidt number. Monotonic increase of  $\Delta T_q^+$  is confirmed.

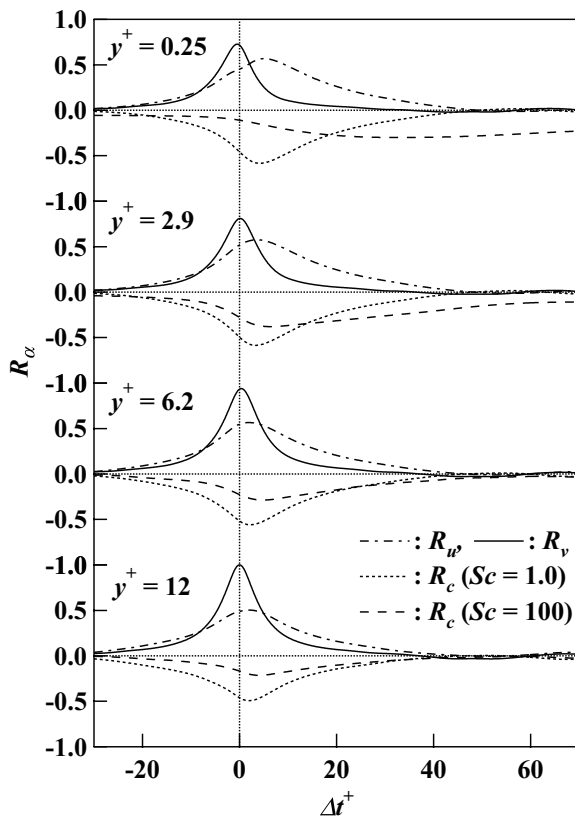


Figure 9: Spatio-temporal correlation between the normal velocity at  $y^+ = 12$  and velocity/concentration fluctuations.

The response time lag at the high Schmidt number also influences the spatial pattern of the local mass transfer rate  $q$ . The instantaneous distributions of  $\gamma$  and  $q$  at  $Sc = 1.0$  and 100 under the identical flow condition are shown in Figs. 12 a) b) and c), respectively. At the low Schmidt number of 1.0, the

low mass-flux regions are characterized by streaky structures, while the high mass-flux regions are spotty, which corresponds to the impingement of bulk fluid (see, dotted areas in Figs. 12 a) and b)). In contrast, at  $Sc = 100$ , both low and high mass flux regions have elongated streaky structures. By carefully comparing Figs. 12 b) and c), it is also observed that the high mass-flux streaks at  $Sc = 100$  lie about  $\Delta x^+ = 200$  downstream of the high mass-flux spots at  $Sc = 1.0$  (see, dotted areas in Figs. 12 b) and c)). Totally, these results are consistent with the spatio-temporal correlation shown in Fig. 10.

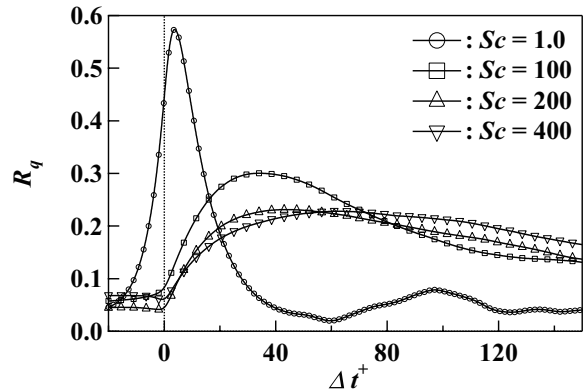


Figure 10: Spatio-temporal correlation between the normal velocity at  $y^+ = 12$  and local mass transfer rate.

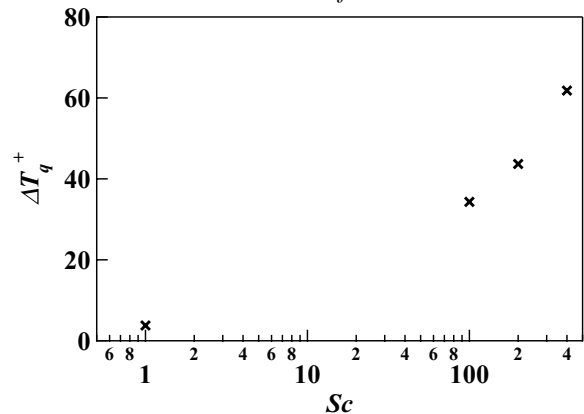


Figure 11: Schmidt number dependency of response time lag of local mass transfer rate

## 6 Conclusions

High Schmidt number effects greatly influence the transport processes inside the viscous sublayer. With increasing the Schmidt number, the high-frequency concentration fluctuations are strongly damped. This trend can be explained by the theoretical analysis by Shaw and Hanratty (1977b). As a result, the concentration field at a higher Schmidt number becomes less sensitive to the velocity fluctuation, and only lower-frequency fluctuations govern the mass transfer. This would be a primary reason why the analogy between the momentum and mass transfer does not hold at high Schmidt numbers. The present results underline the necessity of devel-

oping a mass transfer model taking into account for the damping effect near a solid wall.

### Acknowledgements

The investigations presented in this paper have been obtained within Grant-in-Aid for Young Scientists (B), 19760131 by the Ministry of Education, Culture, Sports, Science and Technology, Japan.

### References

Bergant, R. and Tiselj, I. (2007), Near-wall passive scalar transport at high Prandtl numbers, *Phys. Fluids*, Vol. 19, pp. 065105 1-18.  
Hasegawa, Y. and Kasagi, N. (2008), Systematic analysis of high Schmidt number turbulent mass transfer across clean, contaminated and solid surfaces, *Int. J. Heat Fluid Flow*, to appear.  
Hasegawa, Y. and Kasagi, N. (2007), Effects of interfacial velocity boundary condition on turbulent

mass transfer, *Int. J. Heat Fluid Flow*, Vol. 28, pp. 1192-1203.

Na, Y., Papavassiliou, D.V. and Hanratty, T. (1999), Use of direct numerical simulation to study the effect of Prandtl number on temperature fields, *Int. J. Heat Fluid Flow*, Vol. 20, pp.187-195.

Schwertfirm, F. and Manhart, M. (2007), DNS of passive scalar transport in turbulent channel flow at high Schmidt numbers, *Int. J. Heat Fluid Flow*, Vol. 28, pp. 1204-1214.

Seki, Y., Iwamoto, K. and Kawamura, H. (2006), Prandtl number effect on turbulence quantities through high spatial resolution DNS of turbulent heat transfer in a channel flow, *Proceedings of Turbulence, Heat and Mass Transfer 5*, pp. 301-304.

Shaw, D.A. and Hanratty, T. (1977a), Turbulent mass transfer rates to a wall for large Schmidt number, *A. I. Ch. E. Journal*, Vol. 23, pp. 28-37.

Shaw, D.A. and Hanratty, T. (1977b), Influence of Schmidt number on the fluctuations of turbulent mass transfer to a wall, *A. I. Ch. E. Journal*, Vol. 23, pp. 160-169.

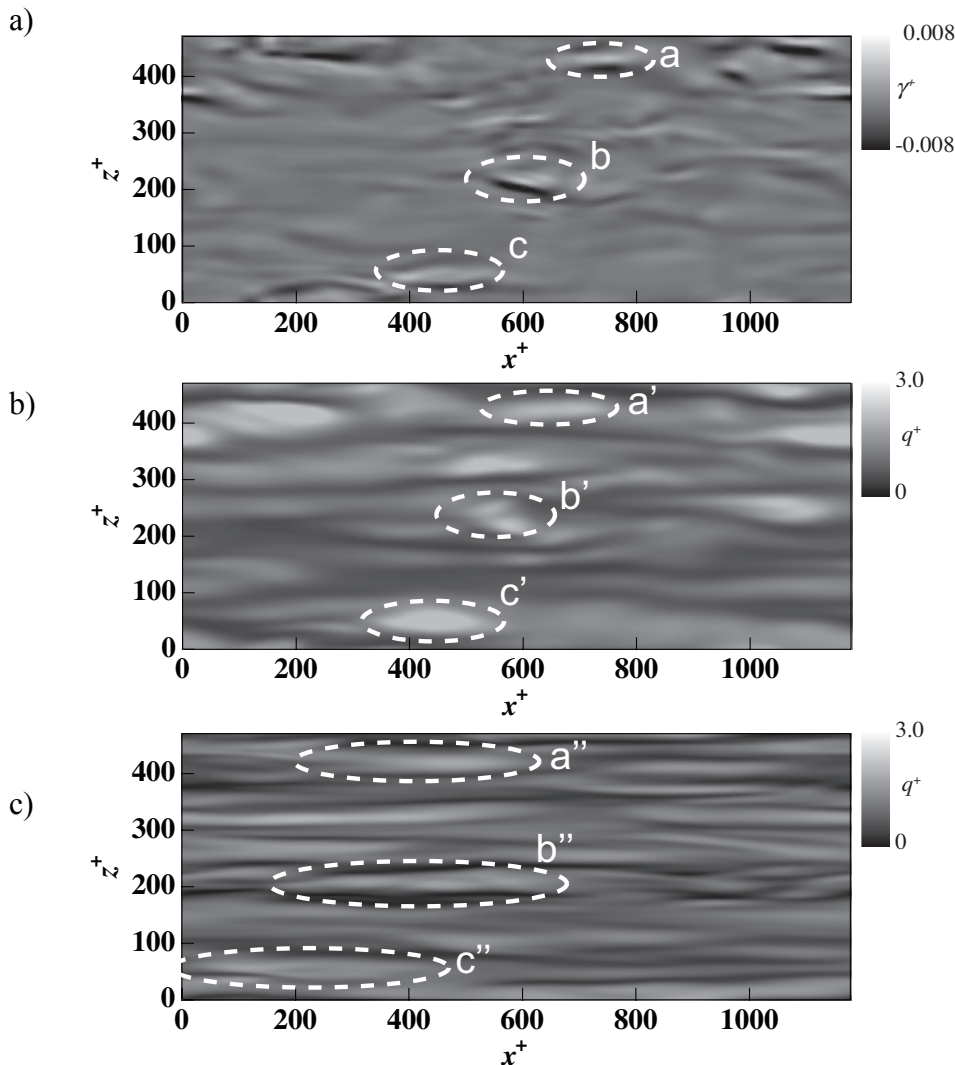


Figure 12: Instantaneous distributions of a)  $\gamma$  and local mass transfer rates  $q$  at b)  $Sc = 1.0$  and c) 100.